HAVSTOVAN
FAROE MARINE RESEARCH INSTITUTE

Monitoring the hydrographic structure of the Faroe Current

Tórshavn · September 2019

Bogi Hansen

Karin Margretha Húsgarð Larsen

Hjálmar Hátún

Kerstin Jochumsen

Svein Østerhus

HAVSTOVAN NR.: 19-02
TECHNICAL REPORT

The present project has been supported by the Danish Energy Agency as part of the Arctic Climate Support Programme. The authors are solely responsible for the results and conclusions presented in the report. They do not necessarily reflect the position of the Danish Energy Agency.

Monitoring the hydrographic structure of the Faroe Current

Bogi Hansen, Karin Margretha Húsgarð Larsen, Hjálmar Hátún, Kerstin Jochumsen, and Svein Østerhus

Abstract

This report is intended as a component in the continuing effort to optimize the system monitoring volume-, heat-, and salt- transports of Atlantic water in the Faroe Current. In this system, the 4°C isotherm is used as the deep boundary of the Atlantic water layer over most of the monitoring section and the main focus of this report is how to monitor the depth of this isotherm with sufficient accuracy in a cost-efficient and sustainable way.

In the established monitoring system, determination of this isotherm depth is mainly based on data from satellite altimetry. The theoretical basis for this relationship is based on geostrophic adjustment of the density field and we discuss how efficient this adjustment is and what uncertainties may be expected in isotherm depth determination with this method. Compared against CTD profiles, the Root-Mean-Square error of this method was found to be between 31 m and 76 m at the various standard stations on the monitoring section, which is between 65% and 92% of the standard deviations of the 4°C isotherm depth. For the monthly averages used in transport time series, the error may be less. When the altimetry data have been updated to include the latest deployment periods, this will be investigated in a study on how to process the historical data set optimally.

Whatever the result of that study, it would clearly be beneficial to have an independent and hopefully more accurate method than altimetry to monitor the depth of the 4°C isotherm on the section. For that purpose, two PIES (Pressure Inverted Echo Sounders) were deployed at two of the CTD standard stations in 2017 and recovered in 2019 in a cooperation between Havstovan and the University of Hamburg. The results from this experiment indicate that a PIES is able to continuously monitor the depth of this isotherm above the PIES location with a Root-Mean-Square error around 30 m, again compared to snapshot CTD observations.

In addition to this, analysis of the historical CTD data set indicates that monitoring isotherm depth at every second standard stations should allow coverage of the whole section by interpolation. We therefore recommend that 3 PIES are acquired and more or less continuously deployed at stations N05, N07, and N09.

1 Introduction

The Faroe Current is the strongest of the flow branches that transport warm and saline Atlantic water into the Nordic Seas and farther into the Arctic Mediterranean. Monitoring the temperature, salinity, and velocity field of this current was initiated more than twenty years ago, but efforts have been ongoing to optimize the monitoring system with a view both to make it more accurate and to make it less dependent on ressource-demanding in situ instrumentation.

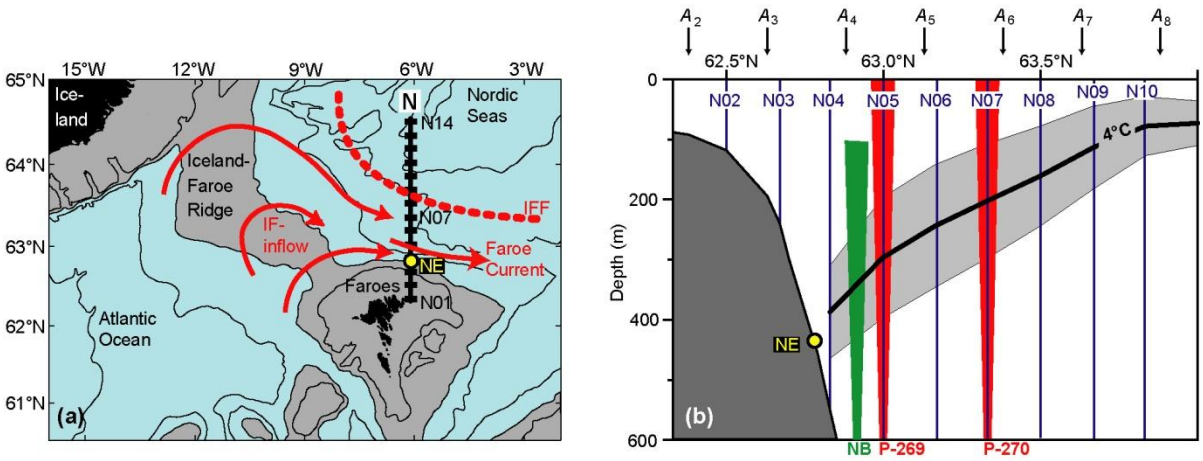

Figure 1. (a) The Iceland-Faroe region with red arrows indicating the Atlantic water inflow to the Nordic Seas between Iceland an Faroes (IF-inflow) and its continuation in the Faroe Current. The thick black line shows the monitoring section, the N-section, with CTD standard stations indicated by black rectangles labelled N01 to N14. **(b)** The monitoring section with the CTD standard stations from N02 to N10 indicated by vertical blue lines and altimetry grid points A_2 to A_8 indicated by arrows. The thick black line shows the average depth of the 4°C isotherm and the grey area indicates its standard deviation. Red cones indicate the two moored PIES. Green cone indicates a long-term ADCP mooring at site NB. In both panels, "NE" indicates bottom temperature monitoring.

The monitoring is carried out on a section, the "N-section" (Figure 1) and has two main components: one to monitor the velocity field, and one to monitor the two hydrographic fields, temperature, and salinity. The velocity monitoring was originally carried out by moored ADCPs, but comparison of ADCP measurements with sea level data from satellite altimetry indicated that altimetry data may in fact give a better representation of the velocity field once they have been calibrated by long-term ADCP measurements (Hansen et al., 2015). This has been verified and for the velocity field, the future monitoring system will mainly rely on altimetry although one ADCP mooring will be retained at a key long-term mooring location (NB, Figure 1b) (Hansen et al., 2019).

This, then, leaves the monitoring of the hydrographic fields as the problem to solve and that is the purpose of this report. This may again be seen as a combination of two tasks. One of these is to monitor the variations and changes of the temperatures and salinities of the water masses that flow through the monitoring section (Figure 1). This task will continue to be realized by regular CTD measurements on the 14 standard stations of the section.

From the CTD data, we can determine the slow variations in water mass properties, which need to be known to derive transports of heat and salt, but also to distinguish the Atlantic water from the other water masses on the section. In addition to these slow variations, there are, however, also more rapid variations as isotherms and isohalines move up or down in various parts of the section. Of special interest is the depth of the 4°C isotherm since this isotherm is used to define the lower boundary of Atlantic water on the section (Hansen et al., 2015). It is the determination of this isotherm depth that is the primay focus of this report.

1.1 Main characteristics of the 4°C isotherm depth along the section

The southernmost part of the section is almost always covered by Atlantic water warmer than 4°C from surface to bottom, but from standard station N04 northward to the Iceland-Faroes Front (IFF on Figure 1a), we generally find the Atlantic water in the top layers with colder and less saline water masses of Arctic origin in the deeper layers. The average depth of the 4°C isotherm for these stations and its standard deviation are listed in Table 1 and illustrated in Figure 1b.

Table 1. Main characteristics of the 4°C isotherm at standard stations on the section based on CTD observations 1987 – 2019. The table lists the number of CTD profiles at each station, the percentage of profiles with surface water being warmer than 4°C, the average depth of the 4°C isotherm and its standard deviation where only occupations with the 4°C isotherm within the CTD profile are included.

Station:	N01	N02	N03	N04	N05	N06	N07	N08	N09	N10	N11	N12	N13	N14
Number CTD:	155	152	142	135	133	120	122	117	116	114	110	100	98	100
Surf > 4°C:	100	100	100	100	98	99	96	91	82	78	75	78	73	79
Avg D_4 (m):				387	297	244	202	161	114	78	73	69	67	65
Std D_4 (m):				77	100	102	95	83	69	49	37	33	30	29

The CTD standard stations are located equidistantly with 10 nautical miles between neighbouring stations and the 4°C isotherm depth does not vary randomly from one station to another. This is documented in Table 2, which shows that the isotherm depths are positively correlated for the whole section with statistical significance of at least 95% ($p < 0.05$). As expected, the highest correlations are found between neighbouring stations, but the 4°C isotherm depth at N04 is not as well correlated with the other stations.

Table 2 The numbers above the diagonal list pairwise correlation between 4°C isotherm depths at the CTD standard stations with statistical significance[1]. Numbers below the diagonal show the number of values for each analysis. Only cruises where CTD profiles were acquired from both stations within 24 hours are included.

	N04	N05	N06	N07	N08	N09	N10
N04		0.56***	0.25**	0.24*	0.20*	0.23*	0.20*
N05	124		0.69***	0.47***	0.31***	0.26**	0.21*
N06	111	119		0.79***	0.36***	0.26**	0.28**
N07	112	118	117		0.66***	0.51***	0.39***
N08	107	113	113	116		0.79***	0.52***
N09	106	112	112	115	112		0.68***
N10	105	111	111	113	111	113	

The high correlations between neighbouring stations in Table 2 indicate that the isotherm depth at one station perhaps may be well approximated by the average depth of the isotherm at the two neighbouring stations and that is indeed the case as shown by the high correlations in Table 3. The last row of the table lists the Root-Mean-Square error in using this method (assuming perfect values at the two neighbouring stations). The high correlations indicate that a system monitoring isotherm depth at every other station accurately might allow determination of the depths at the other stations, as well (not necessarily by averaging).

[1] Here and elsewhere in the report, statistical significance is indicated by asterixes: * means $p < 0.05$. ** means $p < 0.01$. *** means $p < 0.001$. Significance levels of correlation coefficients have been corrected for serial correlation by the modified Chelton method recommended by Pyper and Peterman (1998).

Table 3. Number of CTD cruises (N) and correlation coefficient between the measured 4°C isotherm depth at one station and the average of the isotherm depths at the two neighbouring stations. The last row lists the Root-Mean-Square error made by replacing the measured value by the average. Only cruises where CTD profiles were acquired from all three stations within 24 hours are included.

Station:	N05	N06	N07	N08	N09
No cruises:	108	115	114	112	110
Correlation C.:	0.82***	0.86***	0.89***	0.82***	0.84***
RMS:	48m	40m	35m	40m	28m

1.2 The established monitoring method for the depth of the 4°C isotherm

In the established monitoring system, values for the 4°C isotherm depth are determined from altimetry, using regression equations that were generated by comparison with the CTD data (Hansen et al., 2015). For station N07, the regression equation explains almost two thirds of the variance in isotherm depth (R^2 = 0.65, Table 4) and the Root-Mean-Square error is around two thirds of the standard deviation (Table 1). For the other stations, smaller fractions of the variance are explained, which is most problematic for station N04, close to the core of Atlantic water flow. In periods with bottom temperature logging at site NE (Figure 1), a regression equation using both altimetry and bottom temperature explains more of the variance of 4°C isotherm depth at N04 (R^2 = 0.58).

Table 4. The performance of the established monitoring system for the 4°C isotherm depth, using regression equations with sea level height from altimetry as input. The table lists the "goodness of fit" (R^2) and Root-Mean-Square error (RMS) of the regression equations used to determine isotherm depth. Based on Table 2.4.1 in the supplementary document of Hansen et al. (2015).

Station:	N04	N05	N06	N07	N08	N09	N10	N11
R^2:	0.50	0.56	0.58	0.65	0.62	0.58	0.47	0.42
RMS:	71m	76m	69m	62m	59m	45m	36m	31m

1.3 The aim and structure of this report

From the last row of Table 4, it appears that the uncertainties of the established method for monitoring the 4°C isotherm depth are fairly high. To some extent, this may be misleading, however, since the isotherm depths from CTD profiles and from altimetry have different time scales. As discussed in Sect. 2.2, the decorrelation time of the altimetry values are many days (Figure 3), whereas the CTD profiles are snapshots that may be contaminated by internal waves and other rapid processes. The time series generated by the monitoring system are based on monthly averages (Hansen et al., 2015), for which the high uncertainties in the last row of Table 4 are not necessarily appropriate.

This question might perhaps be somewhat clarified by a comparison of the PIES data discussed in Sect. 3 and altimetry data. Unfortunately, the altimetry data have not been updated for the full PIES deployment period at the time of writing. This is also most relevant when considering how best to process the historic data set and is planned to be treated in a separate report, using all the available data, including altimetry data for the full PIES deployment period when they have been updated in order to optimize the algorithms developed in Hansen et al. (2015).

In this report, we rather focus on how to optimize the future monitoring system and, for that purpose we need to better understand the link between altimetry and isotherm depth and its limitations, which is discussed in Sect. 2. In addition, it would clearly be beneficial to have an independent observational system that can monitor isotherm depth continuously. Due to the heavy fishing activity, traditional moorings are not an option. Instead, we have investigated the possibility of using PIES.

In a cooperation between Havstovan and the University of Hamburg, two PIES were deployed at two of the CTD standard stations on the monitoring section (N05 and N07, Figure 1b) in 2017. They were recovered in June 2019 and seem to have functioned well. The results from this experiment and the potential for using PIES to monitor isotherm depth are discussed in Sect. 3, and Sect. 4 concludes the report with recommendations for the future monitoring system. The two main sections, Sect. 2 and Sect. 3 have been written in different periods and have different nomenclature and different periods of data.

The work reported here has been supported by funding from the Danish Energy Agency in the FARMON and FARMON II projects, as well as the European Union's Horizon 2020 research and innovation programme under grant agreement no. 727852 (Blue-Action).

2 Geostrophic adjustment

2.1 Introduction

It has been noted that there is a fairly tight link between sea level height – as observed by altimetry – and the depth of the 4°C isotherm (Figure 1) on the N-section (Hansen et al., 2015). We interpret this as a baroclinic response of the density field to changes in the barotropic forcing and use the term "geostrophic adjustment" to denote this response.

From a simple theoretical framework, geostrophic adjustment may be seen as the tendency for the ocean to maintain geostrophic balance when affected by slow changes in the barotropic forcing: If the currents in the upper layer of a layered ocean are changing while the deep currents remain constant, then the density field has to change to maintain geostrophic balance.

On the N-section, the deep currents are, however, not constant and to some extent, they seem to co-vary with the upper currents. Furthermore, geostrophic adjustment is generally expected to be slow. Barotropic changes propagate with barotropic waves, which are fast, but baroclinic waves are generally much slower.

Thus, there are a number of questions that need to be answered: How efficient is the geostrophic adjustment ? How fast is it ? what are the processes responsible ? In this Section, we try to address these questions.

2.2 Barotropic and baroclinic pressure variations

The pressure at a certain point in the ocean may be considered as a sum of two contributions, a barotropic pressure p_t and a baroclinic pressure p_c:

$$P(t) = P_t(t) + P_c(t) = g \cdot \rho(0,t) \cdot h(t) + g \cdot \int_{z=0}^{D} \rho(z,t)dz \qquad (1)$$

where z is the vertical coordinate (positive downwards from a fixed level), D the depth of the point below that level, $\rho(z,t)$ the density, and $h(t)$ the height of the sea surface at time t. Since we are mainly interested in variations, we may use the altimetric SLA value for $h(t)$ to get a barotropic pressure anomaly $p_t(t)$ and subtract a constant density ρ_0 from $\rho(z,t)$ (to get a signal with relatively higher variations). Thus, we may define a baroclinic pressure anomaly:

$$p_c(t) = g \cdot \int_{z=0}^{D} (\rho(z,t) - \rho_0)dz \qquad (2)$$

where we will use ρ_0 = 1027.3 kg m^{-3}, which is a typical surface density on the N-section. To check how the baroclinic pressure component reacts to a change in the barotropic pressure component (i.e., sea level), we have calculated lagged correlation coefficients between these two pressure components at 800 m depth on stations N05 to N10 on the N-section using CTD data from 1996 to August 2015. We used altimetry grid points and interpolated in latitude to get SLA values directly above the latitudes of the CTD stations.

We find highly significant correlation coefficients between the barotropic and the baroclinic pressure anomalies (Table 5), so that we can write:

$$p_c(t) = a \cdot p_t(t) + b \quad \Rightarrow \quad p(t) = (1+a) \cdot p_t(t) + b \qquad (3)$$

where a and b may be determined by regression and $p(t)$ is the total pressure anomaly. Table 5 lists values for the regression coefficient, a, for zero lag, a_0, as well as for the lag giving the best correlation, a_m.

Table 5. Correlation and regression coefficients between baroclinic pressure anomaly, Eq. (2), at 800 m depth on standard stations N05 to N10 and the barotropic pressure anomaly. "*N*" is number of values, "Std." is the standard deviation of SLA, "R_0" is the correlation coefficient with lag 0 and "a_0" the corresponding regression coefficient, Eq. (3). "*Lag*" is the lag giving maximum absolute correlation, which is "R_m" and "a_m" is the corresponding regression coefficient. Negative lag means that the barotropic pressure anomaly leads the baroclinic anomaly.

Stat.	*N*	Std.	R_0	a_0	*Lag*	R_m	a_m
N05	87	6.74	-0.77***	-0.85	-1	-0.78	-0.86
N06	79	7.48	-0.77***	-0.78	-1	-0.78	-0.79
N07	82	7.72	-0.84***	-0.78	0	-0.84	-0.78
N08	80	7.47	-0.83***	-0.68	0	-0.83	-0.68
N09	79	7.10	-0.80***	-0.48	2	-0.80	-0.48
N10	79	6.69	-0.67***	-0.33	4	-0.68	-0.34

We might perhaps expect the baroclinic anomaly to lag after the barotropic, which implies negative values for "*Lag*" in Table 5. This is the case for stations N05 and N06, but the lag is only one day. For N07 and N08 there is no lag, and for N09 and N10 it is positive. The lag does not, however, give a large difference in correlation coefficient and the difference is probably not significant. Figure 2 shows a cross-correlation plot for three selected stations.

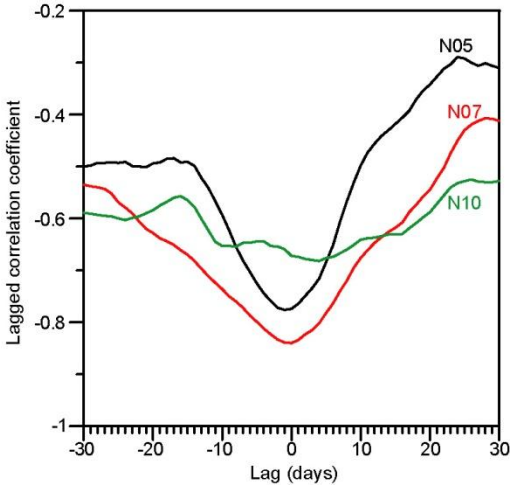

Figure 2. Lagged correlation between barotropic and baroclinic pressure anomalies for three standard stations. Negative lag means that the barotropic pressure anomaly leads the baroclinic anomaly.

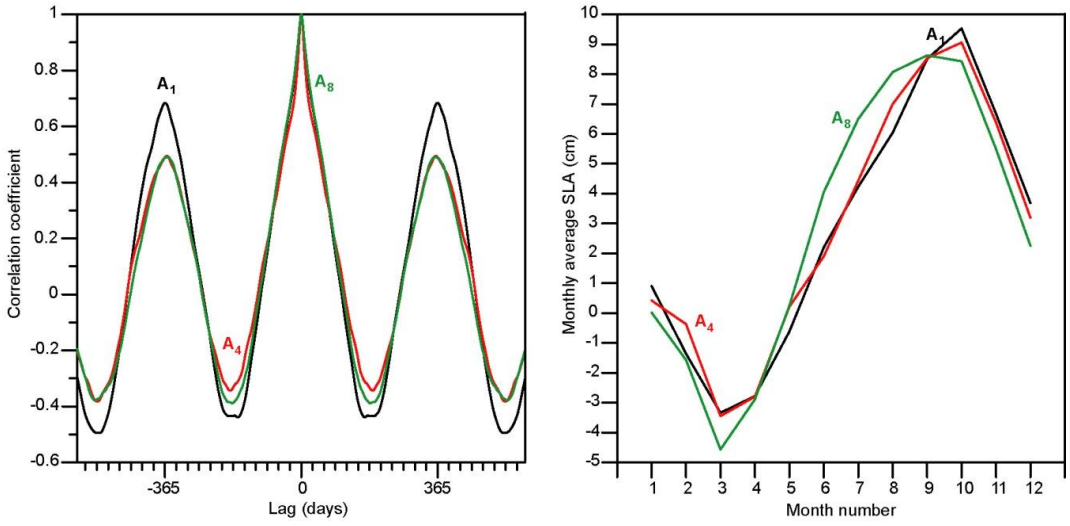

Figure 3. Left panel: Autocorrelation of SLA at three grid points for lags from -600 to +600 days. **Right panel:** Monthly average SLA at the same grid points. The points are: (A_1, 62.125°N, 6.125°W), (A_4, 62.875°N, 6.125°W), (A_8, 63.875°N, 6.125°W). Based on the period 1993 – 2014.

For the innermost stations, Figure 2 shows that the cross-correlation peaks fade off within ±10 to ±20 days. This may be due to the autocorrelation of the SLA values, which has a central peak of the same width whereas the rest of the autocorrelation seems to be dominated by the seasonal signal (Figure 3).

The message from Table 5 seems to be that the baroclinic pressure anomaly responds rapidly to a change in the barotropic anomaly at the innermost innermost stations with almost complete (85%) compensation at N05 and decreasing compensation as we move northwards from the slope. At station N10, it seems as if there is little response to the instantaneous values of the sea level and that most of the variation is seasonal.

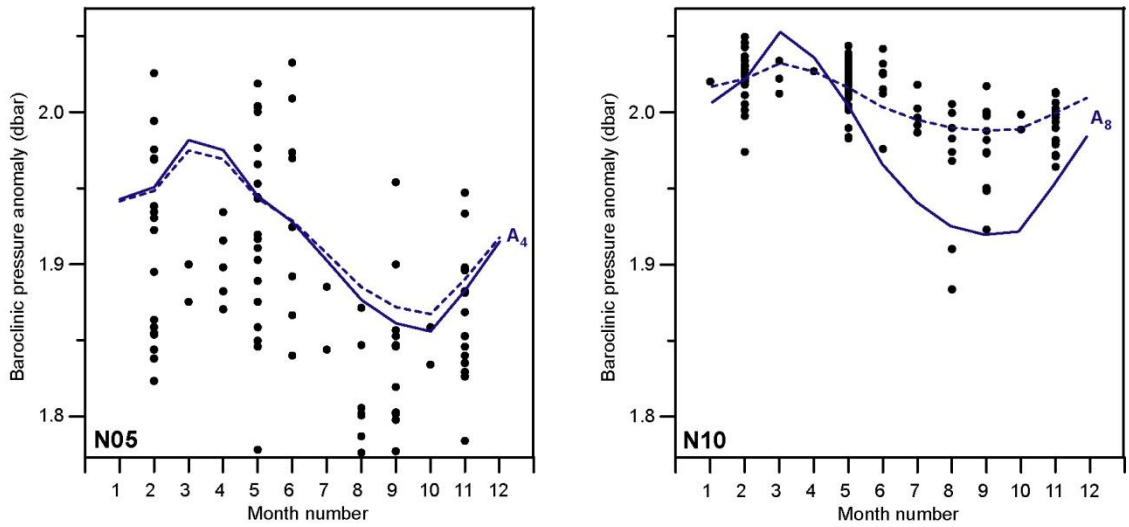

Figure 4. The seasonal variation of the baroclinic pressure anomaly at station N05 (left panel) and N10 (right panel). The continuous blue curves show inverted barotropic pressure anomaly at grid points A_4 (left panel) and A_8 (right panel), close to N05 and N10, respectively, Figure 1) in the same vertical scale (vertical location relative). The dashed curves show the same but with vertical scale multiplied by 0.85 and 0.33, respectively (Table 5).

This is verified in Figure 4. In the left panel (station N05) of that figure, we do see a seasonal signal, but it is almost hidden by the large short-term variations. In the right panel (station N10), in contrast, the baroclinic pressure anomaly varies much less and has a clearer seasonal variation except for a few outliers in summer. The continuous blue curves in the figure show the seasonal variation of the barotropic pressure anomaly from altimetry points A_4 and A_8 (copied from the right panel of Figure 3 appropriately scaled). These curves have been inverted for better comparison and their vertical locations in the figure are arbitrary. The curves have similar seasonal variations as the points but with larger amplitude, especially for N10. This is consistent with regression factors of magnitude less than one (Table 5). To illustrate this, the dashed blue curves show the seasonal altimetry variation multiplied by the respective regression coefficient, again inverted and with arbitrary vertical locations.

2.3 Baroclinic pressure and barotropic velocity

The high correlations for the inner stations in Table 5 demonstrate a tight relationship between baroclinic and barotropic pressure on a daily time scale, which is in reality a relationship between baroclinic pressure and sea level height, *h(t)*, Eq. (1). Geostrophic adjustment should, however, be a response of the density field to the velocity field rather than to sea level and sea level may change from other dauses than from velocity changes. To check this, we may regress the baroclinic pressure anomaly at station N05 on the sea level change across the current (i.e. between N05 and altimetry point A_8, which is located north of the typical current (Figure 1b).

$$p_{c\,N05}(t) = a_d \cdot g \cdot \rho_0 \left(h_{N05}(t) - h_{A_8}(t) \right) + b_d \qquad (4)$$

As seen in Table 6, there is still a significant relationship, but it is much weaker than Eq. (3) since R_d = -0.56 (Table 6) compared to R_0 = -0.77 (Table 5). One reason for this is that we have ignored the seasonal sea level variation, which is almost the same at N05 and A_8 (Figure 3, right panel). If we add the monthly averaged sea level at N05, $h_{Month,N05}(t)$ to the bracket on the right side of Eq. (4), we get Eq. (5), and now the correlation coefficient (R_{ds} in Table 6) has almost the same magnitude as R_0 in Table 5.

$$p_{c\,N05}(t) = a_{ds} \cdot g \cdot \rho_0 \left(h_{N05}(t) - h_{A_8}(t) + h_{Month,N05}(t) \right) + b_{ds} \qquad (5)$$

Table 6. Correlation and regression coefficients between baroclinic pressure anomaly, Eq. (2), at 800 m depth on standard station N05 and the sea level difference between N05 and A_8 as represented by Eq. (4), R_d and a_d, and by Eq. (5), R_{ds} and a_{ds}.

Stat.	*N*	R_d	a_d	R_{ds}	a_{ds}
N05	87	-0.56***	-0.92	-0.72***	-0.79

To a large extent, the high (negative) correlations between barotropic and baroclinic pressure for the inner stations in Table 5 may thus be seen as results of processes occurring over two different temporal (and spatial) scales. The rapid process is geostrophic adjustment of the density field to changes in the barotropic forcing, occurring on daily time scales. In addition to this, the baroclinic pressure is also linked to sea level variations on annual time scales, associated with circulation variations on larger spatial scales.

Other temporal scales enter, as well, but it is remarkable that these two scales explain so much of the variation. There is, however, a fundamental difference between the processes occuring on these two temporal scales. The geostrophic adjustment associated with the daily variations involves vertical movement of isopycnals with convergence or divergence of upper and deeper water masses, but with only minimal changes of the water masses. For the annual variations, in contrast, the upper water mass will vary in density due to seasonal warming and cooling, but the isopycnals in the boundary between upper and deeper water masses may not necessarily move very much vertically.

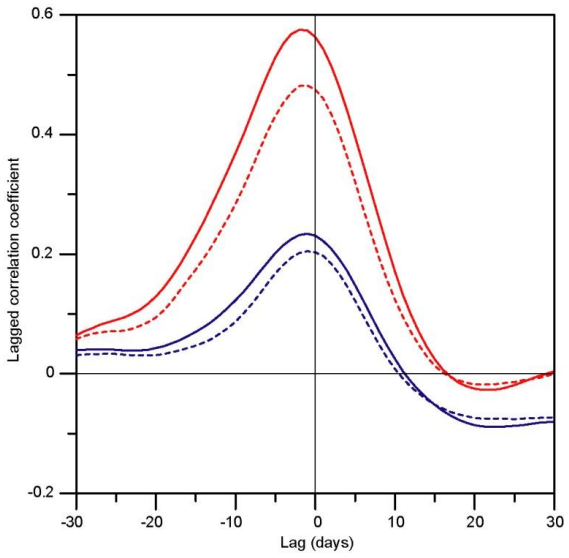

Figure 5. Lagged cross-correlation between bottom temperature at NE and two altimetry parameters. Dashed lines are daily averages. Continuous lines are weekly averages. For blue lines, the altimetry parameter is the SLA value at altimetry grid point A_4. For red lines, the parameter is the difference SLA(A_4)-SLA(A_8). Site NE is at (62.79°N, 6.083°W, 455m bottom depth) that is close to point A_4. Negative lag means that altimetry leads temperature.

While the variations in baroclinic pressure at depth are well explained as responses to sea level variations, Eq. (3), the variations in isopycnal (and isothermal) depths may therefore be better explained by variations in the sea level difference across the current and that seems indeed to be the case as illustrated in Figure 5.

In this figure, the bottom temperature at ADCP site NE (Figure 1) is correlated with altimetry with lags from -30 to +30 days. Warm water at this location implies that the warm (and relatively light) Atlantic layer is deep so that the baroclinic pressure anomaly should be relatively small. We find a positive relationship between altimetry and bottom temperature with negligible lag, but the correlation is much better when we use sea level difference between A_4 and A_8 than using sea level at A_4 only.

2.4 Time scales of geostrophic adjustment

As mentioned in Sect 2.1, geostrophic adjustment is generally considered to be slow, since it is propagated by baroclinic (internal) waves, but both baroclinic pressure at depth (Table 5 and Figure 2) and bottom temperature at NE (Figure 5) seem to respond within a day or so.

To understand this, we may model the Faroe Current as a two-layer system with an average depth of the upper layer of 200 m and a density difference $\Delta\rho \approx 0.5$ kg m^{-3}. The speed of an internal wave will then be on the order of 1 m s^{-1} or ≈100 km per day. From Figure 1, we see that the monitoring section is ≈100 km downstream of the Iceland-Faroe Ridge and it is after crossing the ridge that the water acquires its baroclinic character. If this is the distance that an internal wave has to travel to restore geostrophic balance on the monitoring section, then a response within a day or so is not unrealistic.

3 Estimating isotherm depth from PIES measurements

3.1 Introduction

A PIES (Pressure Inverted Echo Sounder) is an instrument that can measure pressure and the travel time of a sound echo at regular intervals (Figure 6). Since both pressure and the two-way travel time between the PIES and the surface depend on temperature and salinity variations, the PIES measurements may in principle be used to determine essential features of the hydrography in the water column above the PIES.

Figure 6. One of the PIES (P-269) that was used in the experiment. The PIES is mounted on an anchor frame and deployed on the bottom. The measurements are stored in the instrument and may be uploaded to a research vessel acoustically or retrieved after the PIES has been released from the frame and recovered.

For the purpose of monitoring the Faroe Current, we are especially interested in estimating the depth of the 4°C isotherm along the monitoring section. To assess the utility of PIES measurements for this purpose, two PIES (P-269 and P-270) were deployed at two locations, N05 and N07 (Figure 1) in 2017 and recovered in 2019. These two locations are parts of a set of standard CTD stations that have been monitored regularly since the late 1980s and from which we have a large set of CTD profiles. Here, we discuss the results of this experiment and the potential utility of using PIES to monitor the hydrographic structure on the section.

3.2 Combining PIES and CTD data

With a PIES situated at the bottom, the two-way travel time, τ, for a sound pulse to travel from the PIES up to the surface and back again is:

$$\tau(t) = \int_{-\Delta h(t)}^{B} \frac{2}{c(z,t)}\, dz \qquad (6)$$

where B is the depth of the bottom (or more accurately of the PIES sound transducer) below a reference level, Δh is the sea level height above this level, and $c(z,t)$ is the speed of sound at depth z and time t. The speed of sound in seawater is a known function of temperature, T, salinity, S, and pressure, P. From a CTD profile at the site, these parameters are known at meter intervals: T_i, S_i, and P_i, and the travel time, τ_T, due to hydrographic (sound speed) variations ($\Delta h = 0$) may be estimated as:

$$\tau_T \cong \sum_{i=1}^{B} \frac{2}{c(T_i,S_i,P_i)} \qquad (7)$$

Similarly, the bottom pressure, $P_B(t)$, is given by:

$$P_B(t) = P_{Atm} + \int_{-\Delta h(t)}^{B} g \cdot \rho(z,t)dz = P_{Atm} + g \cdot \rho_0 \cdot [B + \Delta h(t)] + \Delta P_B(t) \qquad (8)$$

where P_{Atm} is atmospheric pressure, $\rho_0 = 10^3$ kg m^{-3}, and the bottom pressure anomaly, $\Delta P_B(t)$, is:

$$\Delta P_B(t) = \int_{-\Delta h(t)}^{B} g \cdot \sigma(z,t)dz \cong \sum_{i=1}^{B} g \cdot \sigma(T_i, S_i, P_i) \qquad (9)$$

At both PIES sites, we have more than a hundred CTD profiles. For each of these profiles, we can estimate τ_T and ΔP_B, as well as the depth of the 4°C isotherm, D_4. This should allow us to check whether there are consistent relationships between these parameters. Unfortunately, the CTD profiles seldom reach close to the bottom, but most of them reach a depth of 1281 m. We therefore extrapolate from this depth down to the depth of the two PIES, approximately 1693 m.

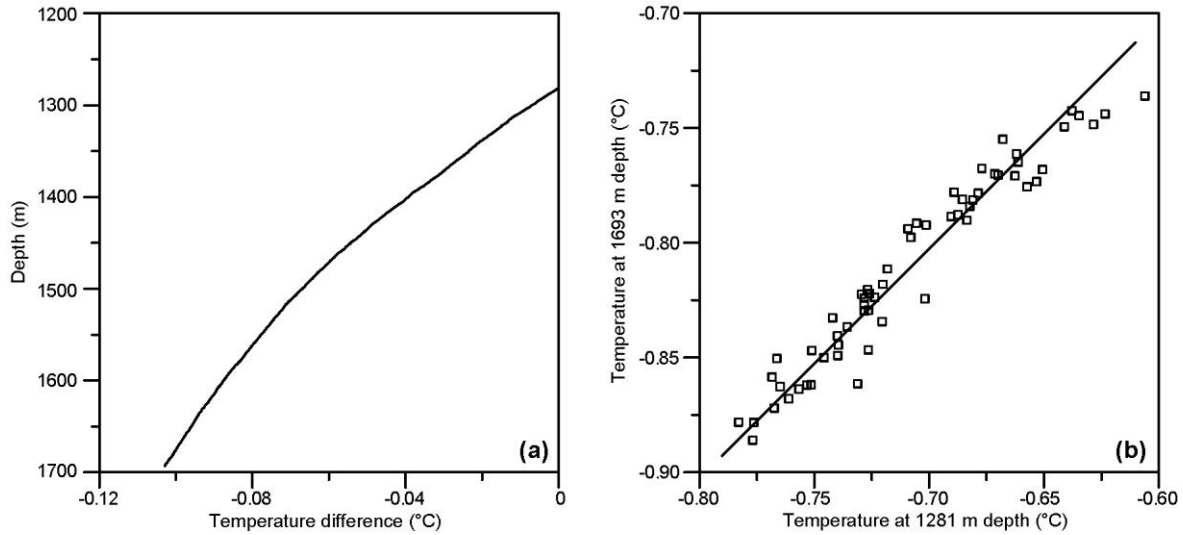

Figure 7. Temperature change with depth at station N14. **(a)** Depth variation of the average temperature difference, $\Delta T_{N14}(z)$. **(b)** Temperature at 1693 m depth plotted against temperature at 1281 m depth for each of 60 CTD profiles. The straight line indicates the temperature at 1693 m depth calculated from the temperature at 1281 m depth, using Eq. (10).

Fortunately, the hydrographic conditions do not change very much below 1281 m and we will assume that the salinity is depth independent in the extrapolation interval. For the temperature in this interval, T(z), we assume that it may be approximated as:

$$T(z) = T(1281m) + \Delta T_{N14}(z) \qquad (10)$$

where $\Delta T_{N14}(z)$ is the average temperature difference at depth z (between 1281m and 1693m) on standard station N14, from which we have 60 CTD profiles that extend at least to 1693 m. The depth variation of $\Delta T_{N14}(z)$ is shown in Figure 7a. As illustrated in Figure 7b, Eq. (10) seems to be a good approximation at station N14. For stations N05 and N07, we do not expect Eq. (10) to be as good, but it seems to be an acceptable way to solve the scarcity of CTD data below 1281 m depth at N05 and N07.

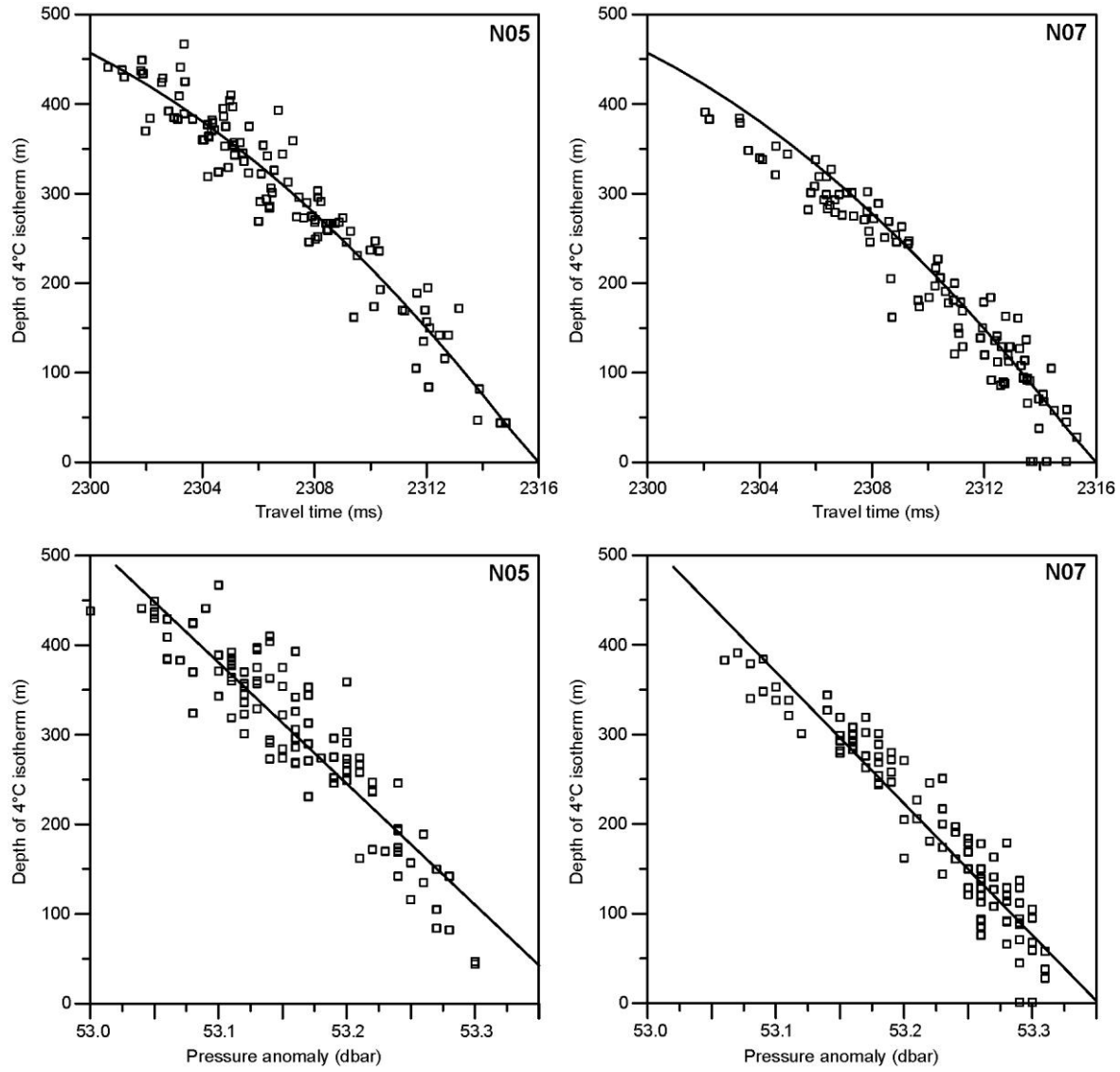

Figure 8. Depth of the 4°C isotherm plotted against travel time (upper panels) and against bottom pressure anomaly (lower panels). Each square represents a CTD profile. Continuous lines indicate the fits: Eq. (11) and Eq. (12).

With this, we can now from each CTD profile at either of the sites (Table 7) calculate the depth of the 4°C isotherm, D_4, as well as the travel time, τ_T, and bottom pressure anomaly, ΔP_B, when sea level variations are ignored. From Figure 8, both τ_T and ΔP_B are related to D_4. To enable the use of these relationships, fits have been established by regression as indicated by the continuous lines in Figure 8. For the relationship between D_4 and τ_T, we have used a second order expression:

$$D_4(t) = \langle D_4 \rangle + \alpha_\tau \cdot (\tau_T(t) - \langle \tau_T \rangle) + \beta_\tau \cdot (\tau_T(t) - \langle \tau_T \rangle)^2 + \gamma_\tau \qquad (11)$$

where, as before, <> indicates averaging. For the relationship between D_4 and ΔP_B, a linear expression was found to be more realistic:

$$D_4(t) = \langle D_4 \rangle + \alpha_P \cdot (\Delta P_B(t) - \langle \Delta P_B \rangle) \qquad (12)$$

For N07, there were 4 profiles, for which all the water column was colder than 4°C. These cases were included in the regressions with $D_4 = 0$. As seen in Table 7, the RMS error was below 30 m for the

relationship between D_4 and τ_T, Eq. (11), and somewhat higher for the relationship between D_4 and ΔP_B, Eq. (12). Extrapolating temperature and salinity from 1281 to 1693 m involves some uncertainty, but a sensitivity analysis indicates that this will be less than 0.1 ms in travel time, equivalent to some 3 m in isotherm depth.

Table 7. For each of the two sites, the table first lists the number of CTD profiles reaching at least 1281 m depth (N) and the average depth of the 4°C isotherm (<D_4>). Then, for each of the fits, Eq. (11) and Eq. (12), are listed the goodness-of-fit (R^2), the average values of the parameters, and the Root-Mean-Square (RMS) errors of the fits.

			Travel time			Bottom pressure anomaly		
Site	N	<D_4>	R^2	<τ_T>	RMS	R^2	<ΔP_B>	RMS
N05	110	298	0.92	2307.0ms	28m	0.84	53.16dbar	40m
N07	103	195	0.93	2310.0ms	27m	0.90	53.22dbar	33m

3.3 The PIES measurements

Each of the PIES measured bottom pressure twice every hour and travel time 24 times every hour. Bottom temperature was also measured twice every hour, but these values were so much biased (several tenths of a degree) that they will not be used further. The two PIES were deployed in 2017, on August 31 at N05, and on October 21 at N07. Both PIES were recovered on June 8, 2019. We will only use data from days with complete coverage (Table 8).

Table 8. PIES data characteristics. For each of the PIES, the table lists the measurement period (days of deployment and of recovery not included), the number of complete days, average values for bottom pressure (P_B) and for travel time (τ), and percentage of values error-flagged for travel time.

Site	YYYY/MM/DD - YYYY/MM/DD	Days	Average P_B	Average τ	Flagged τ
N05	2017/09/01 - 2019/06/07	645	1728.66 dbar	2309.138 ms	3%
N07	2017/10/22 - 2019/06/07	594	1727.58 dbar	2310.167 ms	21%

3.4 PIES bottom pressure data

The raw (half-hourly) bottom pressure values (thin black lines in Figure 9) appear to be of high quality. Both of the PIES seem to have been deployed at almost exactly the same depth, with an average bottom pressure close to 1728 dbar. When we subtract the initial offset, which includes the atmospheric pressure, this corresponds to a depth of 1693 m. We use this depth as a reference depth for the analysis.

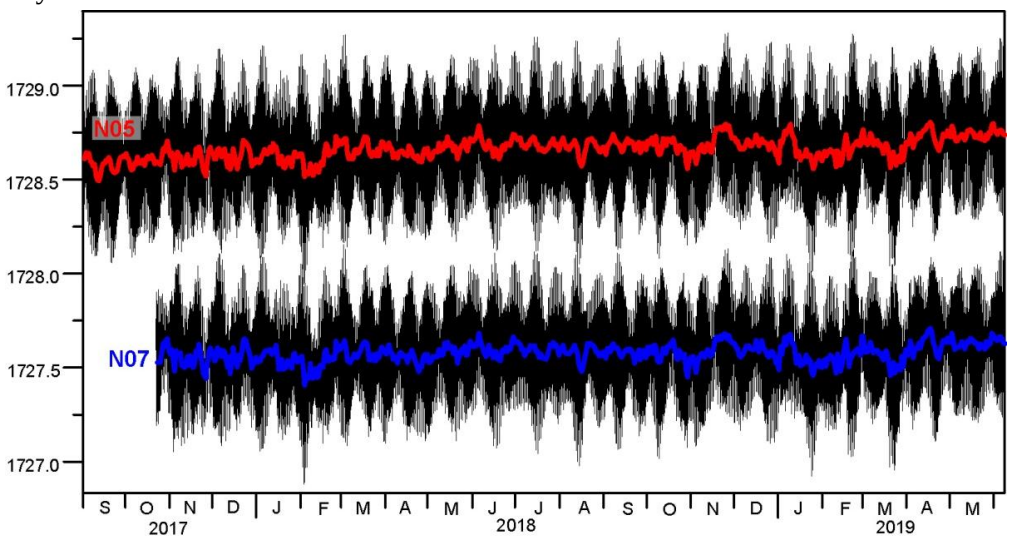

Figure 9. Bottom pressure measured by the two PIES through the deployment period. Thin black lines show raw (half-hourly) values. Thick coloured lines show daily averaged values.

There are clear indications of tidal variations, which is supported by spectral analysis (Figure 10), but there are also indications of trends, especially for N05. A linear trend analysis gave $5.4 \cdot 10^{-3}$ dbar/month for N05 and $2.7 \cdot 10^{-3}$ dbar/month for N07. Both of these values are well within the drift specifications cited and are likely to be of instrumental origin.

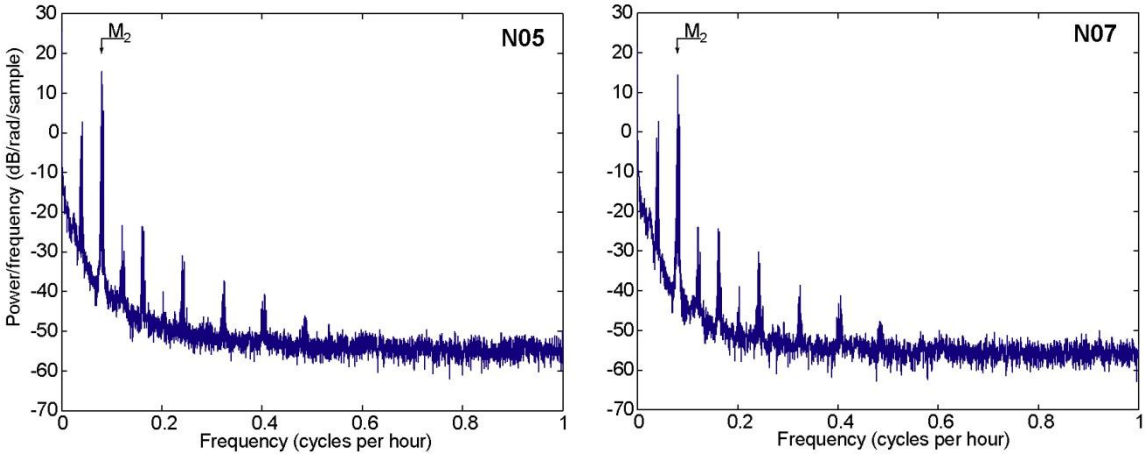

Figure 10. Power spectra of bottom pressure at the two sites using the Welch method (Matlab pwelch function). The highest peak is seen to be located at the frequency of M_2.

Since the trend is likely to be due to instrumental drift, it has been removed, and Figure 11 shows daily averaged de-trended bottom pressure at the two sites. The two curves co-vary extremely well and the correlation coefficient between them is 0.96 ($p < 0.001$).

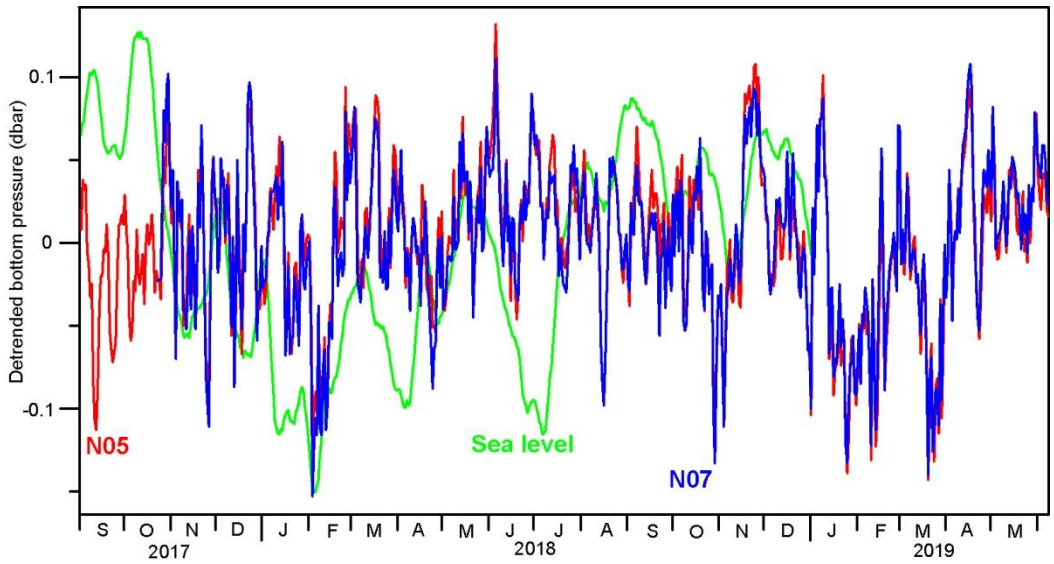

Figure 11. Daily averaged de-trended bottom pressure at site N05 (red curve) and at site N07 (blue curve) plotted together with daily values for sea level height (green curve) from satellite altimetry at altimetry grid point A_5 close to both PIES sites (63.125°N, 6.125°W), scaled such that the pressure variations from sea level are in the same scale as the PIES data. The altimetry data end in December 2018 because they had not been updated for the whole period at the time of processing.

In spite of the pronounced tidal signal in the bottom pressure (Figure 10), the daily averaged de-trended series (red and blue curves in Figure 11) do not resemble the sea level height measurements from satellite altimetry (green curve in Figure 11). This apparent paradox may perhaps be due to

geostrophic adjustment (Sect. 2), which is not sufficiently rapid to destroy the tidal signal, but still fairly efficient at daily time scales.

This indicates that the daily averaged bottom pressure variations in Figure 11 stem from variations in the hydrographic properties of the water column, rather than from sea level variations. In support of this, the range of pressure variations in Figure 11 is of the same magnitude (≈ 0.2 dbar) as the range in the lower panels of Figure 8.

3.5 PIES travel time data

In contrast to the pressure measurements, the measurements of travel time, τ, are clearly contaminated by many errors. From Figure 8, we expect τ to be slightly higher than 2300 ms. This depends, of course, on the depth of the PIES below surface, but even a depth increase of 1 m will only increase τ by a bit more than 1 ms. As shown in the upper panels of Figure 12, both sites have a clear peak in the histogram around this expected value of τ, but a few values are considerably higher and many values are considerably lower, indicating reflection from within the water column, rather than the surface. For both PIES, the number of erroneous values increases with decreasing τ down to the lockout value, which is a time interval after pulse transmission where the receiver is locked out to prevent erroneous values. This lockout time ought probably to have been set higher.

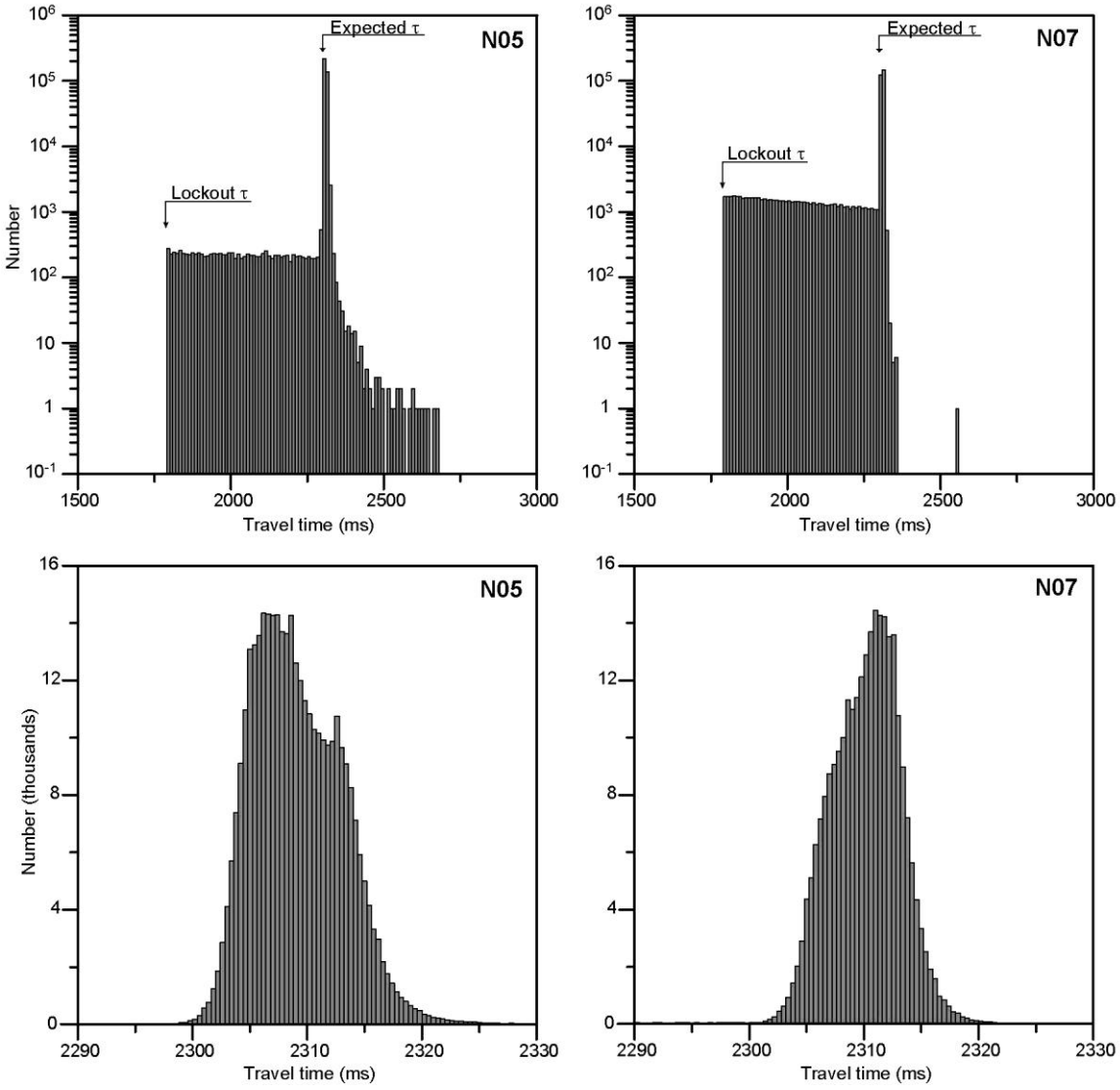

Figure 12. Histograms of travel time measurements by the two PIES for a wide interval (upper panels, note logarithmic scale) and for an interval around the expected values of τ (lower panels, note linear scale). In the upper panels, the lockout time and the expected travel time are indicated.

In spite of the many erroneous values, most of the values for τ are located close to the expected 2300 ms, as demonstrated in the lower panels on Figure 12. For both PIES, the width of the histogram peak is a bit less than 20 ms, which is quite as expected from the upper panels of Figure 8. We have therefore chosen to error flag all values outside the interval from 2295 ms to 2330 ms. For N05, this reduced the data set by 3%, but for N07, 21% had to be flagged (Table 8).

Although N05 according to the bottom pressure was around 1 m deeper than N07 (Figure 9), the travel time for N05 is on average 1 ms lower than for N07 (Table 8 and Figure 12). Again, this emphasizes that the variation in travel time derives more from variation in hydrography than sea level height.

For further analysis, hourly values for travel time were generated by averaging all the values that had not been flagged. In the best case, the average would be based on 24 individual values, but many hours had fewer than 24 non-flagged values. In the complete data set for both PIES, there was only one hour (at N05), for which all 24 measurements had been error-flagged. This value was interpolated between neighbouring hours so that the hourly time series are complete for both PIES.

The high error frequency in the τ data could make the hourly averaged time series suspect and one may wonder about their quality. If the original data were totally random, we would not expect the hourly averaged time series to be serially correlated, but they are. This is illustrated in Figure 13, showing the autocorrelation functions for τ as well as for P_B. For the pressure data, the autocorrelation function shows the typical oscillatory behaviour of a series with strong tidal influence. For travel time, the indication of a tidal component is weak, especially for N05. Consistent with this, power spectra of τ did not indicate any pronounced tidal peaks.

More importantly, the autocorrelation function for τ does not fall rapidly to zero, but remains positive and fairly high up to a lag of two weeks (Figure 13). This indicates that the variations in the data are not random, but reflect real variations to some extent, at least. The averages of all the non-flagged values for τ from the PIES (Table 8) are very similar to the values derived from historical CTD profiles (Table 7). For N07, the comparison is almost exact. For N05, there is a difference of about 2 ms, half of which may be because N05 was about 1 m deeper than N07 (Table 8). The values for average τ in the two tables are, however, averaged over quite different periods, so exact correspondence should not be expected.

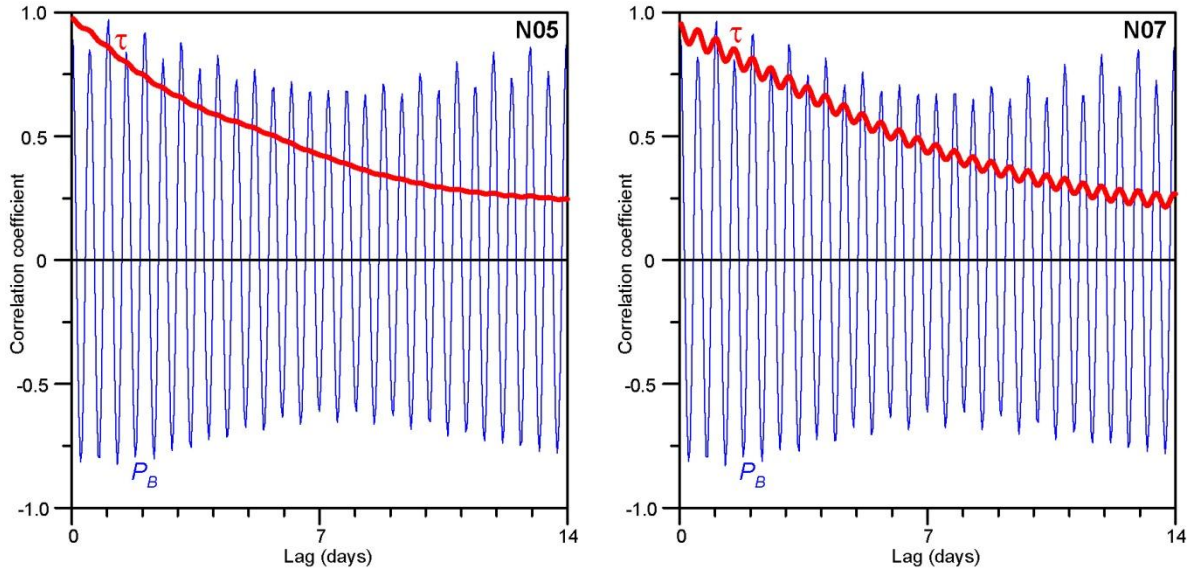

Figure 13. Lagged autocorrelation of travel time (red curves) and bottom pressure (blue curves) for both PIES based on hourly averages.

From the hourly averaged time series, we have generated daily averages (Figure 14). On short time scales, there does not appear to be much coherence between the two daily averaged series, but on longer time scales, the travel times at the two sites do seem to co-vary.

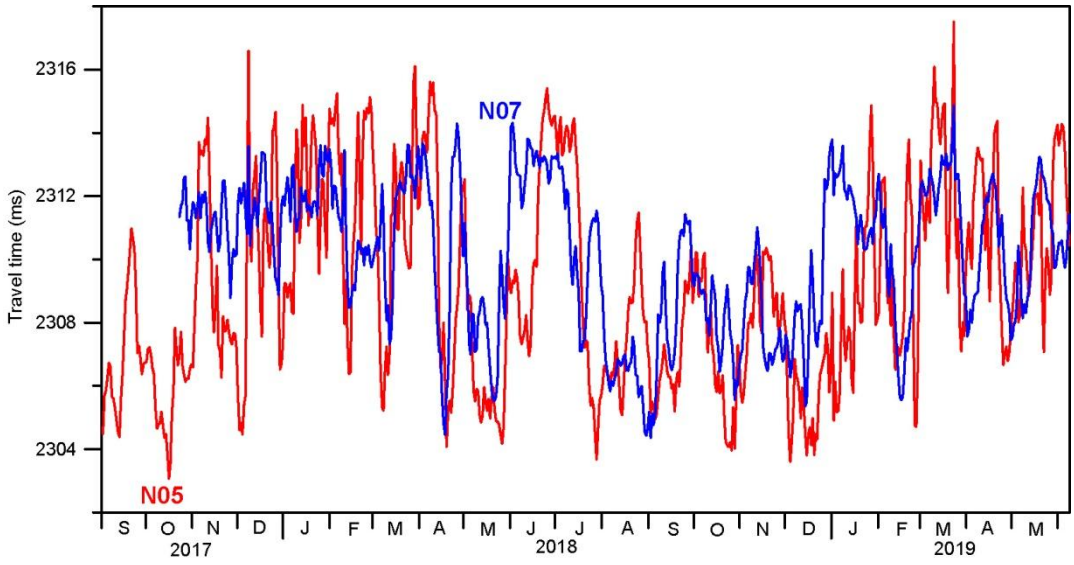

Figure 14. Daily averaged travel time from N05 (red curve) and N07 (blue curve).

3.6 Determination of 4°C isotherm depth from PIES data

The good correspondence between τ values from CTD profiles and the PIES indicates that the relationships determined from the CTD observations may be used to estimate the depth of the 4°C isotherm depth, $D_4(t)$, from PIES data using the relationships in Eq. (11) and Eq. (12). In these equations, the parameters α_τ, β_τ, γ_τ, α_P as well as $\langle D_4 \rangle$ ought to retain their previously determined values (Sect. 3.2). The two averages: $\langle \tau_T \rangle$ and $\langle \Delta P_B \rangle$, on the other hand, depend critically on the exact depths of the two PIES, but we should be able to determine those from the CTD profiles that were obtained from the two sites during the PIES deployment period.

During this period, there were four CTD cruises (Table 9) that have been calibrated and processed so that the travel time, τ_T, may be calculated by Eq. (7). These values are listed in Table 9 together with the average travel time for the same day measured by the PIES, τ_P. With no noise from sea level variations, perfect theory and measurements, the difference between these two values, $\delta\tau = \tau_P - \tau_T$, ought to be constant and reflect real depth relative to the reference depth of 1693 m. As seen in Table 9, these values are not constant, but they vary considerably less than the individual travel time values with the largest deviations from the average δτ being around 0.6 ms at both sites.

Table 9. Calibration of PIES travel time. The table first lists cruise number (Cru.) and date of CTD profiles. Then for each of the sites, it shows station number (St.N), the travel time, τ_T, calculated from the CTD profiles using Eq. (7) with B = 1693 m, the average travel time measured by the PIES for the day of the profile, τ_P, and the difference between the two, δτ.

				Calibration data for N05				Calibration data for N07			
Cru.	YYYY	MM	DD	St.N	τ_T(ms)	τ_P(ms)	δτ(ms)	St.N	τ_T(ms)	τ_P(ms)	δτ(ms)
1802	2018	02	12	8	2303.38	2306.37	2.99	10	2308.06	2308.47	0.41
1821	2018	05	14	10	2301.84	2305.50	3.66	8	2306.94	2307.93	0.99
1838	2018	08	30	9	2304.57	2307.16	2.59	11	2304.00	2304.64	0.64
1902	2019	02	16	41	2304.44	2307.59	3.15	43	2304.09	2305.64	1.55
					Average δτ for N05:		3.10		Average δτ for N07:		0.90

Instead of using daily averaged travel time, we could have used the travel time measured during the hour of the CTD profile for calibration, but these data will be contaminated by tidal variations to a higher degree and attempts to do this gave less consistent values for δτ than Table 9. Thus we will use Eq. (11) with $< \tau_T >$ = (2307.0 + 3.1) ms = 2310.1 ms for N05 and $< \tau_T >$ = (2310.0 + 0.9) ms = 2310.9 ms for N07.

Similarly, the CTD data from the four cruises may be used to calibrate the bottom pressure data for use in Eq. (12), but since the trends (Figure 9) are likely to be due to instrumental drift, we de-trend the pressure series first:

$$P_B^*(t) = P_B(t) - \varepsilon \cdot (t - t_0) \qquad (13)$$

where ε is the trend established by linear regression and t_0 is the start of the deployment period (September 1, 2017). If we ignore variations of sea level (Δh = 0) and atmospheric pressure (P_{Atm} = 10.13 dbar), Eq. (8) may be rewritten as:

$$P_B^*(t) = P_{Atm} + g \cdot \rho_0 \cdot B + \Delta P_B(t) \equiv \delta P + \Delta P_B(t) \qquad (14)$$

We may then use the four CTD cruises in the deployment period to determine δP for each of the PIES (Table 10) and Eq. (12) may be rewritten as:

$$D_4(t) = \langle D_4 \rangle + \alpha_P \cdot (P_B^*(t) - \delta P - \langle \Delta P_B \rangle) \equiv \langle D_4 \rangle + \alpha_P \cdot (P_B^*(t) - \langle P_B^* \rangle) \qquad (15)$$

where the values for $<\Delta P_B>$ are those in Table 7. Using this equation with δP given by the averages in Table 10 would seem to be the best way to determine isotherm depth from bottom pressure, but it should be noted that the values for δP vary considerably from one CTD cruise to another. Thus, we should not expect the results from using Eq. (15) to be very accurate.

Table 10. Calibration of PIES bottom pressure. The table first lists cruise number (Cru.) and date of CTD profiles. Then for each of the sites, it shows station number (St.N), the bottom pressure anomaly, ΔP_B , calculated from the CTD profiles using Eq. (9) with B = 1693 m, the de-trended average bottom pressure measured by the PIES for the day of the profile, P_B*, and the difference between the two, δP.

				Calibration data for N05			Calibration data for N07			
Cru.	YYYY	MM	DD	St.N	ΔP_B	P_B*	δP	St.N	ΔP_B	P_B*	δP
1802	2018	02	12	8	53.082	1728.510	1675.428	10	53.186	1727.447	1674.261
1821	2018	05	14	10	53.054	1728.645	1675.591	8	53.167	1727.583	1674.416
1838	2018	08	30	9	53.079	1728.607	1675.528	11	53.075	1727.551	1674.476
1902	2019	02	16	41	53.108	1728.643	1675.535	43	53.098	1727.602	1674.504
				Average δP for N05:			1675.521	Average δP for N07:			1674.414

With this information, we can finally use the PIES measurements to make two independent estimates of D_4 for each day of the deployment period, one based on travel time, and the other on pressure. For this purpose, we use Eq. (11) and Eq. (15) with the parameters in Table 11.

Table 11. Parameters to be used with Eq. (11) and Eq. (15) to calculate the depth of the 4°C isotherm, D_4, based on PIES measurements at the two sites.

		Travel time				Pressure	
Site	$<D_4>$	$<\tau_T>$	α_τ	β_τ	γ_τ	$<P_B^*>$	α_P
N05	298.1	2310.10	-27.19	-0.813	9.1	1728.68	-1352
N07	194.9	2310.90	-30.06	-0.901	10.4	1727.63	-1468

To assess the quality of these estimates, we may again use CTD data from the four cruises listed in Table 9 and Table 10. In addition, there are two CTD profiles at N05 and one at N07 from cruises (cruises 1919 and 1920) that had not been finally calibrated, but sufficiently to estimate D_4. The result is illustrated in Figure 15, where red squares show D_4 estimated from PIES travel time while the blue squares show D_4 estimated from PIES pressure.

One immediate conclusion from Figure 15 is that the isotherm depths based on the PIES pressure measurements are of little use. The high variations of δP in Table 10 already indicate that there might be a large bias in these estimates, but even taking that into account, there seems to be no consistent relationship between D_4 determined from CTD profiles and D_4 estimated from PIES pressure. This may be due to the noise induced by tidal variations (Figure 9) or variations in sea level and/or atmospheric pressure and future measurements and analysis might conceivably lead to a different result. Here, we can only conclude that the D_4 estimates based on PIES pressure measurements from our analysis are not reliable and will not be discussed further.

For the D_4 estimates based on travel time measurements (red squares in Figure 15), the result is much better. The largest discrepancy between the two D_4 estimates is 56 m for N05 (cruise 1838) and 59 m for N07 (cruise 1919). The Root-Mean-Square error was 31 m for N05 and 35 m for N07. Comparing these values to the RMS values in Table 7, we conclude that only a small part of the error derives from uncertainties of the travel time measurements. Rather, the error seems to derive mainly from the variability in the relationship between D_4 and τ_T, i.e. the deviations of the squares from the lines in the upper panels of Figure 8.

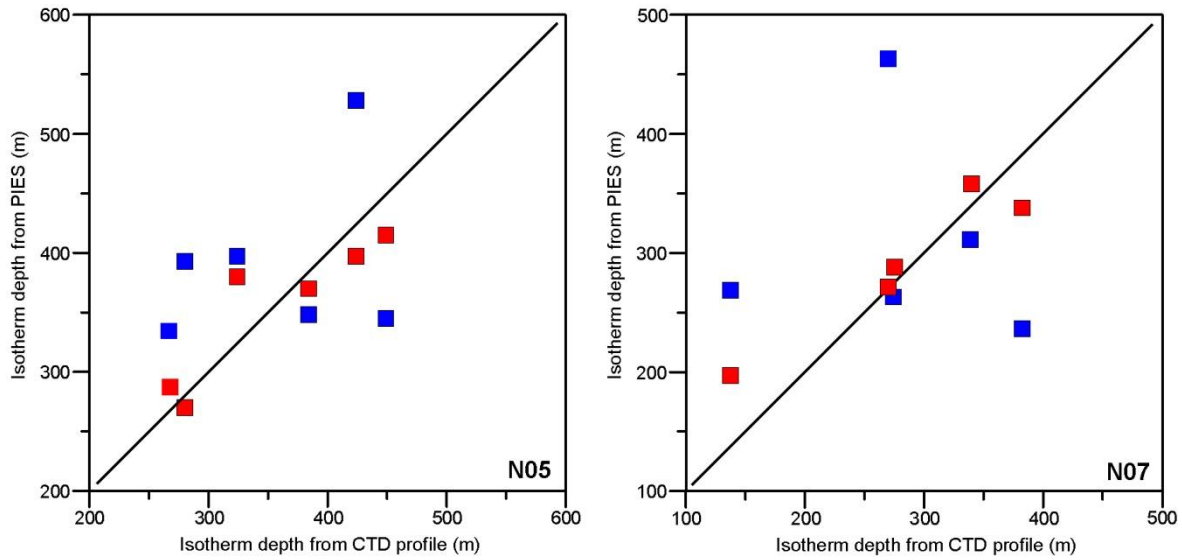

Figure 15. Comparison between 4°C isotherm depth as observed by CTD and as calculated from PIES travel time (red squares) and pressure (blue squares). The diagonal lines indicate equality.

As a consistency check, the values in Table 9 and Table 10 may be used to derive more exact values for the depth of the PIES. From Table 9, the PIES at N05 was sufficiently deeper than 1693 m to give an extra travel time of 3.1 ms, which is equivalent to 2.3 m. From this, the acoustic transducer of the PIES at this site was at a depth of 1695.3 m. From Table 10, we similarly conclude that on average, $P_{Atm} + g \cdot B \cdot \rho_0 = 1675.521$ dbar, which implies $B = 1695.9$ m. Since the pressure sensor is located 58 cm below the acoustic transducer, these two different depth estimates fit perfectly. For N07, we get a depth of 1693.7 m from travel time and 1694.8 m from pressure, which is not quite as good, but still quite acceptable when taking into account the specified accuracy and drift of the pressure sensor.

Except for the three extra profiles from cruises 1919 and 1920, the same CTD profiles have been used for calibration and validation, which detracts from the positive impression of the red squares on Figure 15. It is, however, only the average value for τ_T that is used for calibration, reducing the number of degrees of freedom only by one for each site. Before a final verdict can be made on the validity of this method for determination of isotherm depth, a higher number of CTD profiles need to be acquired during a future deployment phase and hopefully profiles that span the total range of D_4 variation (Figure 8).

Nevertheless, the results from this experiment are encouraging and we may use them to estimate the temporal variations of isotherm depth at the two sites during the deployment period (Figure 16). To a large extent, the 4°C isotherms at the two sites seem to co-vary in depth and both of them appear to co-vary with the sea level height at the altimetry grid point that is located between them (A_5 in Figure 1b). Note that sea level height is positive upwards, whereas depth is positive downwards, and note the difference in scales. Thus, when sea level rises by 20 cm, the 4°C isotherms deepen by a distance that is almost a thousand times greater. This is again an example of geostrophic adjustment (Sect. 2).

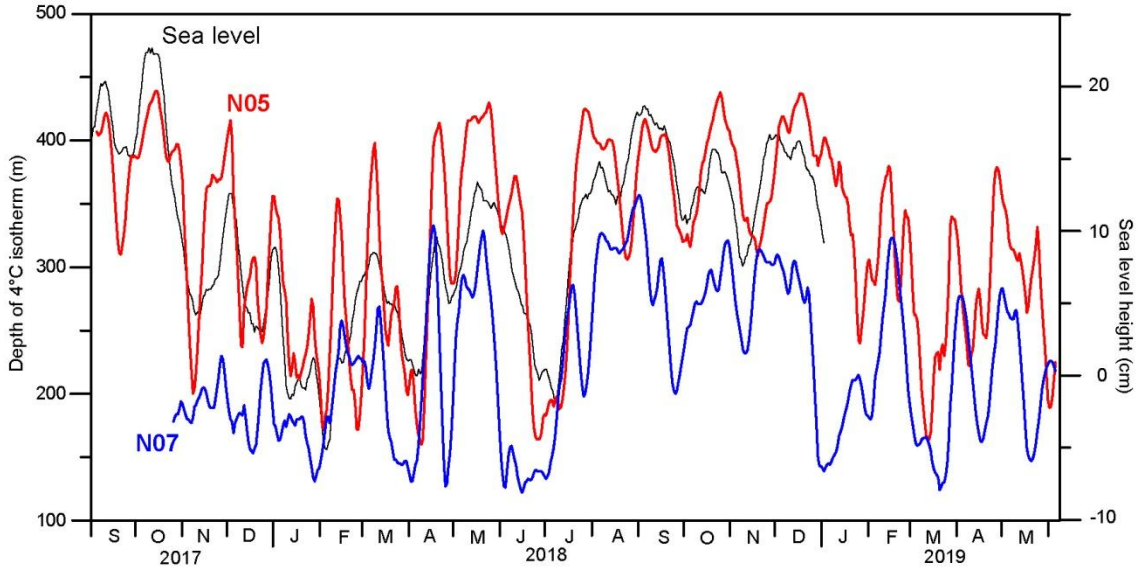

Figure 16. Weekly averaged (running mean) depth of the 4°C isotherm at N05 (red curve, left scale) and N07 (blue curve, left scale) based on PIES travel time measurements plotted together with daily values for sea level height (black curve, right scale) from satellite altimetry at an altimetry grid point between both PIES sites (63.125°N, 6.125°W).

3.7 Discussion

Based on the analysis presented, we find that the pressure measurements of the PIES are not easily utilized to estimate isotherm depth, although this question ought to be re-addressed if a more comprehensive data set can be acquired. The measurements of travel time, on the other hand, seem to allow us to estimate the depth of the 4°C isotherm with an RMS error of around 30 m for both N05 and N07. A caveat is that the number of CTD profiles during the PIES deployment period is rather low to give this value a good statistical significance.

4 Recommendations for the monitoring system

As discussed in the introduction, the main drawback of the existing monitoring system is that sea level data from altimetry are the only observational tool for continuous monitoring of the depth of the 4°C isotherm, used as lower boundary for the Atlantic water on the monitoring section. The background for this technique is geostrophic adjustment, as discussed in Sect. 2, but the adjustment is not perfect and the uncertainty seems to be fairly high (Table 4), although it may possibly be smaller for monthly averages (Sect. 1.3).

From Sect. 3, it appears that PIES are able to monitor the depth of the 4°C isotherm with an uncertainty on the order of 30 m with respect to CTD measurements and possibly more accurately for monthly averages. From Table 3, it furthermore appears that monitoring every second standard station (from N05 northwards) should be sufficient. We therefore recommend that:

- Three PIES are deployed at stations N05, N07, and N09.
- If acoustic uploading of PIES data is found to function well, the PIES should remain on the bottom as long as possible (depending on battery capacity).
- For each PIES deployment, the lockout time should be better adjusted to the expected depth to reduce the number of "bad" echoes.
- For each PIES deployment, a larger number of CTD profiles (at least 10) should be acquired at the deployment site and they should reach as close to the bottom as possible.
- If logistically possible, PIES deployment at each site should overlap for a sufficiently long period to allow inter-calibration.

In addition to this, it may become necessary to establish special monitoring of the isotherm depth at station N04. This station is close to the high-velocity core and has a deep Atlantic water layer. Thus, high quality monitoring at this site is essential, but the station is so shallow that a PIES on the bottom would be vulnerable to fisheries. There are, however, several observational parameters (altimetry, bottom temperature at NE, ADCP velocity profile at NB, PIES at N05) that perhaps may be combined to give adequate monitoring. When the altimetry data have been updated to cover the full PIES deployment period, this question will be addressed.

References

Hansen, B., Larsen, K. M. H., Hátún, H., Kristiansen, R., Mortensen, E., and Østerhus, S.: Transport of volume, heat, and salt towards the Arctic in the Faroe Current 1993–2013, Ocean Sci., 11, 743–757, https://doi.org/10.5194/os-11-743-2015, 2015.

Hansen, B., Larsen, K. M. H., and Hátún, H.: Monitoring the velocity structure of the Faroe Current. Havstovan Technical Report 19-01, May 2019.

Pyper, B. J. and Peterman, R. M.: Comparison of methods to account for autocorrelation in correlation analyses of fish data, Can. J. Fish. Aquat. Sci., 55, 2127–2140, https://doi.org/10.1139/f98-104, 1998.

P.O. Box 3051 · Nóatún 1
FO-110 Tórshavn
Faroe Islands

Tel +298 35 39 00
hav@hav.fo
www.hav.fo